Lift-off performance of electromagnetic acoustic transducers (EMATs) for surface acoustic wave generation

L. Xiang, S. Dixon, C. B. Thring, Z. Li, R. S. Edwards

Department of Physics, University of Warwick, Coventry CV4 7AL, United Kingdom,

Abstract

Electromagnetic acoustic transducers (EMATs) have a behaviour that depends on the distance between the transducer and the surface of the material under test, namely the lift-off. Rayleigh waves generated by EMATs suffer from waveform distortion as the lift-off is increased. This paper describes this distortion numerically and experimentally, focusing on the spatial distribution of the induced currents and hence the ultrasound pulses. This is verified experimentally using an EMAT consisting of a magnet and a single 1.5 mm wide linear coil, showing a decrease in peak frequency for the wideband Rayleigh wave of the order of 100 kHz/mm with lift-off. The behaviour when using EMATs in an array configuration (equivalent to a meander-coil, where the current through neighbouring coils is in opposite directions) is then described. Coil spacing is shown to affect the lift-off behaviour, with the spatial model predicting well the frequency behaviour. The lift-off behaviours of physically spaced coils and those which are pulsed with time delays to give an effective separation are shown to be equivalent for all but the smallest separations; unless very small separations are required to give a high frequency signal, the effective spatial current distribution spread for a single coil counteracts the benefits of reducing the dipole effect. Good performance with lift-off variation is hard to achieve at high frequency, and lift-off must be considered if a particular frequency of operation is required.

Keywords: Ultrasonics, arrays, EMAT, Lift-off, Rayleigh surface wave

1. Introduction

Electromagnetic acoustic transducers (EMATs) are an established non-contact ultrasonic transducer, primarily used in the field of non-destructive testing (NDT) [1]. An EMAT generally consists of a permanent magnet (or electro-magnet) to introduce a static field, and a coil to introduce a dynamic electromagnetic field within the skin depth of a conductive material. For non-magnetic materials, such as the aluminium samples used within this work, transduction is purely via the Lorentz force mechanism [1, 2]. Generation and detection of ultrasonic modes depend on the configuration of the EMAT coil and magnet(s). The coupling between the electromagnetic and elastic fields is strongly affected by the distance between the EMAT and the material surface, namely the lift-off [3]. An EMAT can be operated at a small lift-off from the sample (normally within a few millimetres, depending on the transducer design, frequency of operation, wavemode used, and the driving electronics). EMATs in industry are suitable for operation in harsh conditions [4, 5], and can be used for fast scanning e.g. on railway tracks [6]. Surface acoustic waves, such as Rayleigh waves, can be used for material

Email address: r.s.edwards@warwick.ac.uk (R. S. Edwards)

characterisation and surface-crack inspection/sizing. This can consider the transmitted signal amplitude or frequency content, and hence any changes in frequency with lift-off are of importance [6].

The behaviour of EMATs with increasing lift-off is an important issue when considering their applications. The lift-off plays a significant role in the generation process, as it not only lowers the transduction efficiency but also varies the coil effective inductance. Clark et al. [7] showed that the change in impedance with lift-off causes a phase shift in the output voltage, which leads to errors on velocity measurements [8]. Huang et al. considered similar behaviour for the magnetostrictive generation mechanism [9]. Increased lift-off also changes the generated signal amplitude, and can lead to a frequency shift in the generated signals [8, 10]. To improve performance with lift-off, Shi et al. made an impedance matching circuit between the EMAT coil and the pulser to compensate for the the coil electrical variation effect due to the lift-off operation, leading to an improved signal [11]. An alternative approach was to increase lift-off of the permanent magnet, but not the coil, such that the variation in signal amplitude was less extreme during scanning where there are lift-off variations [12].

Studies of the impedance effect [7, 8] illustrate the distortion of the generated ultrasound waveform, which is a consequence of the changing behaviour of the EMAT-material system due to the lift-off. To fully understand the distortion, one must also consider the influence of the dimensional size of the coil and the spatial profile of the induced currents, alongside the electrical behaviour. Jian et al. considered primarily the electrical behaviour with lift-off, producing an equivalent circuit model [13]. The Lorentz force was considered as having two parts; a spatial and a time-dependent force, with the work concentrating on the time dependence and the electrical behaviour.

Many different coil and magnet configurations have been suggested for EMATs. For generation of Rayleigh (surface) waves, a linear or racetrack coil design can give a broadband signal [14]. Where a narrowband signal is preferred, for example for increasing signal amplitude at higher lift-off, a meander-coil

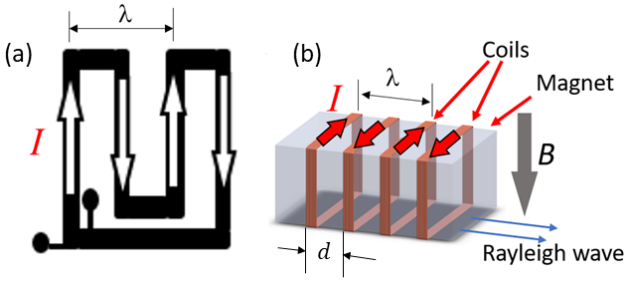

Figure 1: (a) Top-down view of a meander coil design. (b) 4-coil EMAT array, giving pseudo-meander behaviour.

design is an alternative [6, 15–17]. A schematic of a simple meander coil is shown in figure 1(a). In this coil design multiple turns are present, with the currents in opposite directions in neighbouring turns (shown by the white arrows) and the natural wavelength of the coil defined in the figure.Recently, arrays of coils have been suggested as an alternative to a meander coil in order to generate a narrowband signal with a chosen wavelength (shown in figure 1(b)) [18]. The coils can be operated such that the currents in neighbouring coils are in opposite directions, mimicking the meander coil, or with the currents in the same direction [19]. The coils can be activated at the same time, giving a dominant wavelength determined by the physical coil spacing d, or at different times, to give a chosen effective spacing (wavelength), as discussed in reference [18]. A simple version of the array shown in figure 1(b), with two coils with currents in opposite directions to mimic the meander coil, is used in this work.

Despite there being several studies of the effect of lift-off of EMATs on generation of ultrasound, they have all primarily considered a single linear or spiral coil for wideband generation. This work considers the ultrasonic behaviour when a single linear coil, or multiple coils in an array design to mimic a meander coil, are used for generation. Section 2 describes a calculation of the mirror current induced in a non-magnetic sample when the EMAT coil is within a small lift-off from the sample, and demonstrates that this is distorted spatially as lift-off is increased. The effect of this distortion on the generated wave is predicted. Where a meander coil or an array are used, one must

consider first the distortion of the signals generated by each array element or meander turn, and then the interaction between the generated waves, when calculating the lift-off behaviour. Section 3 introduces the experimental set-up used in this work. Section 4 gives a comparison between the theoretical predictions from Section 2, which consider only the spatial effects, and the experimental results. This shows that the spatial effect has a considerable effect on the lift-off behaviour, and must be considered alongside the electrical behaviour.

2. EMAT source fields with lift-off

The influence of the distribution of the EMAT induced Lorentz force field on generation is quantified by considering the underlying electromagnetic coupling between the EMAT coil and the material [1]. An EMAT coil is usually flat with a single layer of wire. A number of studies have calculated the field distribution generated by alternating current (AC) driven coils for various coil geometries, considering the coil shape, orientation, and the tilt angle of the coil relative to the metal surface [1, 3, 20–23].

In this paper, we first demonstrate operation of a simple linear generation coil, with the basic model implemented with the coil held above a linear, homogeneous and conductive material. Figure 2 shows the schematic diagram for the EMAT coil (not including the permanent magnet), consisting of several copper wires, in close proximity to a conducting material. A surrounding time-varying magnetic field (shown by dashed lines, not to scale) is generated by the current pulse through the coil, and this penetrates into the material surface skin depth to form a magnetic field, $\mathbf{H}^M$, where M refers to the fact that this is within the material. A secondary electrical field, namely the mirror current (or eddy-current) $\mathbf{J_e}$, is induced in the material by this time-varying magnetic field. A secondary magnetic field that is associated with $\mathbf{J_e}$ will in turn be created to oppose the primary magnetic field. The secondary field and the mutual effect between the primary and secondary magnetic fields are not considered in this paper, because the current pulse has a very low amplitude of around 50 A and aluminium samples are used, and hence both will be small [24]. They should be considered when analysing the coil electrical characteristics, but have minimal effect on the spatial behaviour considered here.

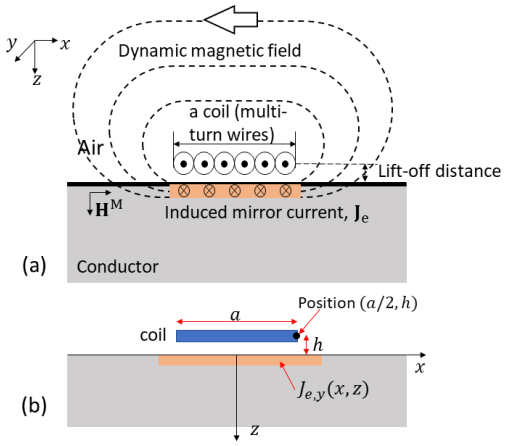

Figure 2: (a) The transient electromagnetic fields generated using the EMAT coil. The dashed lines show the direction of the dynamic magnetic field surrounding the coil. A second electrical field (mirror currents) is induced in the material. Secondary magnetic field and the mutual effect between primary and secondary fields are not indicated. (b) Calculation model of (a).

The ultrasound generated depends on the Lorentz force,

$$\mathbf{F}^{(L)} = \mathbf{J_e} \times \mathbf{B}, \tag{1}$$

where the magnetic field $\mathbf{B}$ includes the dynamic (due to the current pulse) and static (from the permanent magnet) magnetic fields. For generation currents which are relatively small, the dynamic magnetic field can be ignored.

In the two-dimensional space domain (the $x-z$ plane) shown in figure 2(a), the mirror current can be calculated using Maxwell's equations, as in reference [1]. The induced secondary currents in the y-direction (into the page) are given by

$$J_{e,y} = \frac{\partial H_x^M}{\partial z} - \frac{\partial H_z^M}{\partial x}, \tag{2}$$

where H_x^M and H_z^M are the horizontal and vertical components of the dynamic magnetic field in the material's skin depth [1, 18]. The H_z^M term is typically

neglected as it is only really significant at the edges of the coil, and is approximated as zero under the coil.

The EMAT coil can be approximated as a very thin sheet of current of width a centred at the origin, with the electrical charge in the (x, z) plane assumed to be evenly distributed between $(-a/2, h)$ and $(+a/2, h)$, where h is the lift-off between coil and sample, as shown in figure 2(b). Based on this approximation, the component $H_x^M(x, z)$ has been calculated in references [1, 18]. The dynamic magnetic field leads to a current in the y-direction that can be calculated using

$$J_{e,y}(x, z) \approx \frac{\partial H_x^M(x, z)}{\partial z}, \tag{3}$$

giving

$$J_{e,y}(x, z) \propto \quad e^{-(1+i)z/\delta} \times \left[\arctan\left(\frac{x + a/2}{h}\right) - \arctan\left(\frac{x - a/2}{h}\right)\right], \tag{4}$$

with full details in references [1, 18]. The above expression shows that the distribution of $J_{e,y}$ induced in the y-direction depends on the position (x, z) within the material, but also depends on the coil geometry and its location, given by (a, h). The skin depth $\delta = \sqrt{2/\omega\mu\sigma}$ depends on the inducing current oscillation frequency ω, the material permeability μ and conductivity σ. Note that this follows the methods outlined in reference [1] where the time variation is omitted from the calculations. The eddy current contains an extra factor of ω due to the eddy current being related to the time differential of the dynamic magnetic field [25], but this is omitted in this work as it will have a limited effect on the spatial behaviour.

$J_{e,y}$ will exponentially decay with distance into the sample. For typical ultrasonic frequencies in metals, the effective region over which there is a non-negligible $J_{e,y}$ is relatively thin. The coil field of the EMAT can therefore be approximated by calculating the total mirror current contribution over all depths,

$$\tilde{J}_{e,y}(x) = \int_{z=0}^{z=\infty} J_e(x, z)dz \propto \left[\arctan\left(\frac{x + a/2}{h}\right) - \arctan\left(\frac{x - a/2}{h}\right)\right]. \tag{5}$$

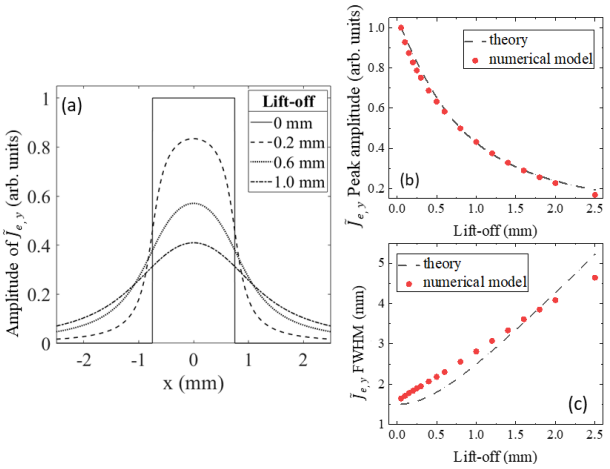

Figure 3: (a). The changing profile of the EMAT induced mirror currents with lift-off from equation 5, for a frequency of 487 kHz. (b)&(c) Comparisons between the COMSOL modelling and the theoretical calculation.

This allows one to simplify the distribution of mirror current from a two-dimensional (xz-plane) description to a one-dimensional (x-axis) problem. Note that z is taken as positive into the sample, as defined in figure 2.

2.1. Spatial distortion of the induced eddy current with lift-off changes

Equation 5 was used to calculate the spatial behaviour of the mirror current as the lift-off was increased. Since a practical EMAT coil is a finite rather than a point source, the mirror current will experience a visible distortion when the lift-off is increased by the same order of magnitude as the coil width, as described by equation 4. An example is given in figure 3(a) to show the change of $\tilde{J}_{e,y}$ for a coil with a width of a =1.5 mm. Lift-off was varied between 0.005 and 1 mm. The mirror current exhibits a significant change as lift-off is increased, with the current intensity dropping and the profile of the induced mirror current broadened.

Numerical modelling was performed to validate the behaviour of $\tilde{J}_{e,y}$ for a more realistic set-up. COMSOL MultiPhysics 5.5 was used to model the EMAT coil in two dimensions. The modelled coil consisted of

seven turns of wire, each with a diameter of 0.2 mm, giving a total width for the coil of 1.5 mm when including a small physical gap between each wire. Aluminium was chosen as the testpiece, with dimensions of 15.0×5.0 mm (width×thickness). The frequency of the current was 487 kHz, chosen to match a frequency where the ultrasound experiments gave a good signal to noise ratio. The lift-off of the coil was varied from 0 to 2.5 mm. The total eddy current density within the material was found and recorded at each lift-off.

Figures 3(b) and (c) show the results for the theory (equation 5, black points) and the COMSOL numerical model (red points). Two parameters, the peak amplitude and the full width half maximum (FWHM) of the current density are plotted. Good agreement is seen between the predictions and the numerical modelling, particularly in the peak amplitude. The FWHM shows a small discrepancy, due to the simplifications of the analytical model which assumes the current profile is a single rectangular block of current, while the COMSOL model considers multiple wires. Despite this small discrepancy, over the practically usable lift-off range of the EMAT there is reasonably good agreement, and the current amplitude and spatial behaviour are the primary considerations when interpreting the lift-off behaviour. Therefore the simplified model described by equation 5 is used for comparison with the experimental data as it offers ease of interpretation of the behaviour.

2.2. Model for Rayleigh surface wave generation

2.2.1. Single coil EMAT

The generation of surface waves using single coil EMATs has been described previously using the coupling between the EMAT source field and the lattice [1, 24]. For the 2D model in figure 2(b), with a large static magnetic field directed into the sample ($B_{0,z}$), and assuming that the current is small enough that the dynamic magnetic field can be ignored, the Lorentz force (equation 1) can be considered using scalars for simplicity. Only the x-component needs to be calculated:

$$\mathbf{F}^{(L)} \approx \mathbf{F}_s^{(L)} = F_s^{(L)} \vec{\boldsymbol{i}}, \tag{6}$$

where $F_s^{(L)}$ is the magnitude of the Lorentz force generated by the static magnetic field and the mirror current. Combining equations 1, 5 and 6 gives

$$F_s^{(L)}(x) = \tilde{J}_{e,y}(x)\ B_{0,z}. \tag{7}$$

If the static field is treated as a constant, the Lorentz force magnitude is proportional to $\tilde{J}_{e,y}(x)$, and the *spatial profile* of the EMAT force is identical to that of the mirror current generated. The generated force due to the static field is then in-plane. The approximation of the static magnetic field as being constant is not true when lift-off is changed; however, the primary effect is a reduction in field at the surface which will affect the amplitude of the generated ultrasound waves, but not the frequency behaviour.

The surface displacement $s(t)$ can be measured as a function of time at a point P, and is a convolution between the temporal driving function $y(t)$ and the spatial profile of the coil [19, 24]. Where there are multiple wires in a coil, each separate piece of wire can be treated as a single line source, and a linear sum of the contributions from each line source gives the final detected ultrasonic displacement signal [14, 19]. For Rayleigh wave generation, one can consider the phase lag between each generated signal, and convert the spatial signal, which is a function of x, to one written as a function of time t, by using $t = x/c_R$, where c_R is the phase velocity of the Rayleigh wave. The spatial profile is described by equation 7, and hence the measured displacement can be written as

$$s(t) \propto \tilde{J}_{e,y}(t(x)) \otimes y(t), \tag{8}$$

where $\otimes$ denotes convolution, and $y(t)$ indicates the driving signal of the EMAT coil (input current).

Equation 8 forms the central theoretical basis of this work. It shows that the behaviour of the generated Rayleigh wave depends on the mirror current distribution, which is affected by lift-off, and the driving current signal temporal behaviour. To evaluate the distortion of the EMAT field, broadband signals for the EMAT driving current were used for all lift-off analysis.

The prediction for ultrasonic generation using a single coil is shown in figure 4. This uses $\tilde{J}_{e,y}$ as shown in figure 3 for a coil positioned at the origin

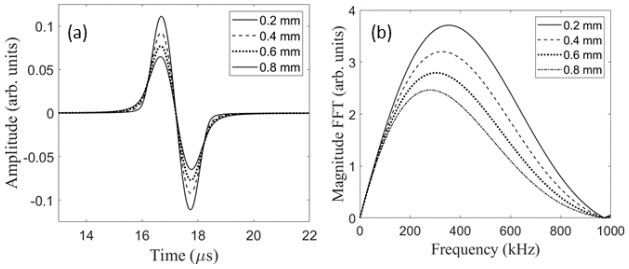

Figure 4: Prediction of the generated ultrasound signals using a single coil, activated at 487 kHz. The coil parameters are the same as in figure 3. (a) Predicted signal in the time domain. (b) Frequency spectrum of (a).

.

with a width of a=1.5 mm. The simulated driving signal was a single-cycle sinusoidal wave, centred at 487 kHz. Figures 4(a) and (b) show the behaviour calculated using equation 8 in both the time and the frequency domain for h from 0.2 to 0.8 mm. Similarly to the spatial change of $\tilde{J}_{e,y}$ with lift-off, the generated ultrasound also experiences a waveform broadening. The corresponding frequency spectrum shows that not only is the amplitude reduced with increasing lift-off, but the peak frequency in the fast Fourier transform (FFT) is also decreased. This phenomenon is very important for consideration when designing experiments to operate at a chosen frequency [14].

2.2.2. Two-coil EMAT

The simplest form of a coil array (or a meander coil) is considered in this section as an array formed of two identical linear coils, with the currents in each coil oriented in opposite directions [15, 18], as shown in figure 1(b) but for two coils only. The two coils are separated by a distance d and are located symmetrically about the origin, with each having the same lift-off (h) value. The induced mirror currents from each of the coils can be represented as $\tilde{J}_{e,y}(x - d/2)$ for the left hand coil, and $\tilde{J}_{e,y}(x + d/2)$ for the right hand coil. Assuming that the two coils are driven simultaneously by the same current, the total current field will be

$$\tilde{J}^{tot}_{e,y} = \tilde{J}_{e,y}(x - d/2) - \tilde{J}_{e,y}(x + d/2), \qquad (9)$$

where the '-' sign indicates that two coils are polarised out-of-phase with each other.

Figures 5(a)-(e), upper panels, show calculations of the spatial behaviour of the current using equation 9 (red solid lines), with the behaviour for a single coil centred on the origin (black dashed lines) shown for comparison. The coils had $a = 1.5$ mm and coil spacing $d = 2.0$ mm, giving a small gap between the two coils. The upper panel shows $\tilde{J}^{tot}_{e,y}$ after normalisation, such that the single coil behaviour has a peak value of 1 at each lift-off. The profile at zero lift-off is close to a square wave, while it becomes closer to a dipole at higher lift-offs.

The data was transformed into the time domain using a Rayleigh wave velocity of 2906 m/s [26] and an FFT was performed, with the results shown in the lower panel of figures 5(a)-(e). If the generation currents were delta functions, one could apply the simple equation $\lambda = 2d$ along with the Rayleigh wave velocity to predict an optimal frequency of operation of 727 kHz. However, a square wave will always give a lower dominant frequency in its spectrum, and the finite width of the coils will also have an effect [14]. The spatial behaviour suggests an optimal frequency of operation of 625 kHz, corresponding to the peak in the FFT at zero lift-off.

The prediction for ultrasonic generation using two coils from equation 8 is given in figures 5(f) and (g) in the time and frequency domains respectively. The driving signal was a single cycle centred at 625 kHz, optimised to the predicted peak value. The overall shape of the time domain waveform is maintained during the increase of lift-off, but an elongation is observed alongside a reduction in amplitude. The corresponding frequency behaviour exhibits a decrease in the peak frequency, which is similar to the behaviour of the single coil.

For a meander coil, a small separation between each coil element allows for generation of surface waves with a high frequency, which is beneficial for detection of small cracks. However, the eddy-current cross-talk underneath the coils will lead to a decreased lift-off performance. The separation d of the coils will therefore have an effect on the measured lift-off behaviour. Models were calculated using different values of d and h for $a = 1.5$ mm. The value of

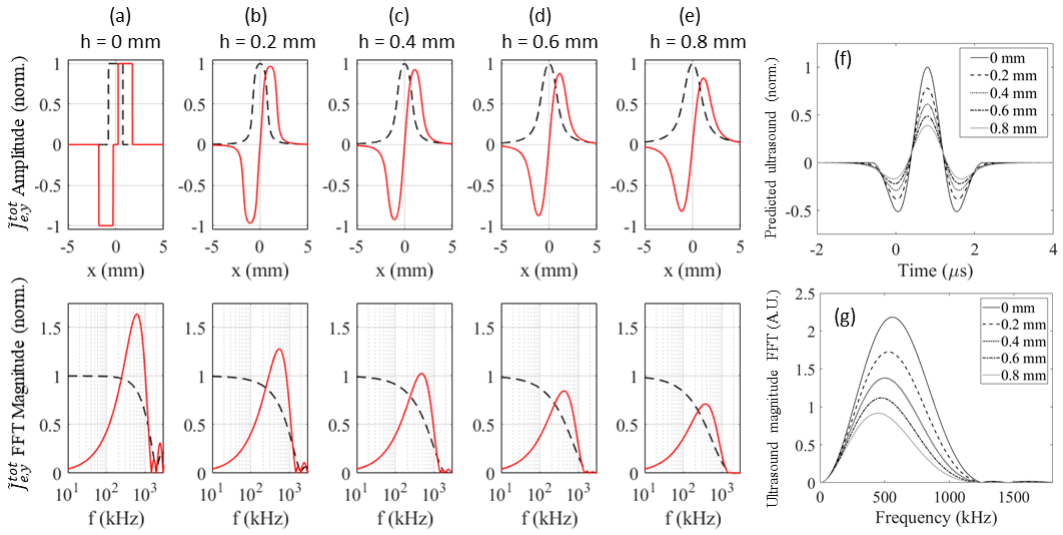

Figure 5: Generation using two coils. (a) to (e) show the lift-off behaviour of the two-coil model (solid red lines) compared to that for a single coil at the origin (dashed lines), with spatial (upper) and frequency (lower) behaviour shown for three lift-offs. (f) and (g) are the predicted ultrasound signals using equation 8 for the two-coil model. The model was created by using two of the models shown in figure 2 separated by a chosen distance.

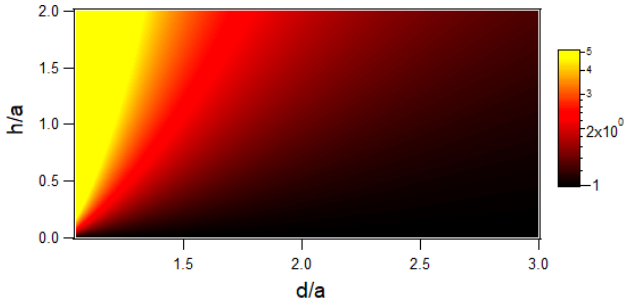

Figure 6: Colour scale plot showing the value of R as lift-off and coil separation is varied. The lift-off effect on the distortion of the signal is strongest for small coil separations.

$\tilde{J}_{e,y}^{tot}$ will always be zero at the centre of the two coils ($x = 0$). To quantify the distortion of the signals, the values of $\tilde{J}_{e,y}^{tot}$ at each edge of the right hand coil were compared; at zero lift-off these will be the same, but will change by different amounts as lift-off is increased if there is any spatial interaction between the generated currents from each coil. A factor R given by

$$R(a,d,h) = \frac{\tilde{J}_{e,y}^{tot}|_{x=d/2+a/2}}{\tilde{J}_{e,y}^{tot}|_{x=d/2-a/2}}, \tag{10}$$

was defined and is plotted in figure 6, where the lift-off and separation are normalised by the coil width a. A value of 1 (black on the colour scale) corresponds to no distortion, meaning the selected coil profile remains the same without influence from its neighbour. The R value drastically increases as d decreases and h increases, showing that the effect of lift-off on the generated ultrasound signals will be strongest for small coil separations.

2.2.3. The equivalence of physical and phased separation of coils

For a meander coil EMAT, or the arrays shown in figure 1, the total ultrasound signal needs to consider the contribution from each turn in the meander, or each coil in the array. Where there are N elements (turns or array coils), with coil j centred at a position x_j, the detected signal can be calculated by taking a sum over all the contributions. Assuming that each element is activated by a signal with the same properties (central frequency, number of cycles) at the same time, described by $y(t)$, the total displacement at the detection point is given by

$$S(t) \propto \left[\sum_{j=1}^{N} \tilde{J}_{e,y}(x + x_j)\right] \otimes y(t), \qquad (11)$$

where $\tilde{J}_{e,y}$ is the current from each coil. For a two-coil system with a separation of d the sum part of this equation simplifies to the same form as equation 9.

Using multiple coils in an array EMAT, as shown in figure 1(b), can give significant benefits for NDT, such as improvement of the signal-to-noise ratio (SNR), and enabling mode/wavelength selectivity of surface acoustic waves [18, 19, 27]. In reference [18], multiple coils were driven at set times using a chosen delay sequence (i.e. were phased) to generate a Rayleigh wave. This allowed the coils to have one physical separation, but behave as if they were at different locations. The effective coil separation in the array is governed by the physical separation and the delay on activation of each coil, which controls the distance that the wave which is generated by the coil activated first travels relative to the second coil before the second coil is activated.

The total signal generated by a phased linear array, when the jth coil is individually controlled by a temporal function $y(t-t_j)$, where t_j is the fixed delay for the jth coil, is given by

$$S_p(t) \propto \sum_{j=1}^{N} \left[\tilde{J}_{e,y}(x + x_j^0) \otimes y(t - t_j)\right] \qquad (12)$$

where x_j^0 denotes the physical location for the jth coil in the array. By using the properties of the convolution function, it can be shown that

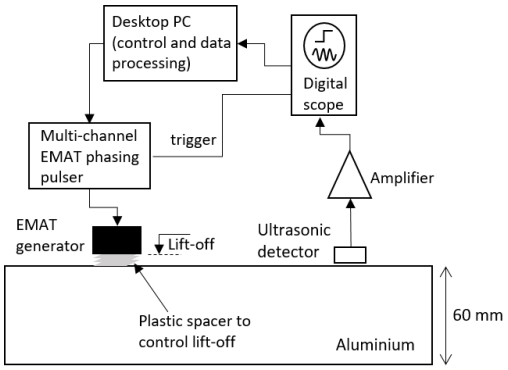

Figure 7: Schematic diagram showing the experimental set-up.

$$S_p(t) \propto \left[\sum_{j=1}^{N} \tilde{J}_{e,y}(x + x_j^0 - t_j c_R)\right] \otimes y(t), \qquad (13)$$

where the effective coil location is now given by $x_j^0 - t_j c_R$. If $x_j^0 - t_j c_R = x_j$ from equation 11, i.e. we compare the behaviour at a phased separation to the equivalent physical separation, the two equations would be equivalent mathematically, and the lift-off behaviour should be the same. Any difference in behaviour would be due to electrical differences between the two set-ups, which would be expected to dominate for whichever out of the phased and physical array had the smallest physical separation, and any differences in magnetic field orientation at each coil.

3. Experimental details

3.1. Multichannel EMAT driver

An in-house built four-channel-output pulser was used to drive the EMATs [18]. The four channels can be individually controlled and are able to deliver either broadband (a single-cycle signal) or narrowband pulses (multiple cycles). The time delay between activating each EMAT coil can be varied in 5 ns steps. The centre frequency can be tuned from 10 kHz to 10 MHz and the maximum voltage output of each channel is 600 V. Details of the driving signals for different tests (single-coil, two-coil, phased two-coil etc.) will be given in the relevant sections.

Two non-contact ultrasonic detectors were used to capture the generated Rayleigh signal. A broadband IntOpSys laser interferometer was first used to measure the out-of-plane displacement signals generated by the single coil EMAT [28]. A racetrack EMAT detector was used to measure the signals generated by two EMAT coils. The effective bandwidth of the EMAT detector was from 0 to 4 MHz [14].

The detected ultrasound signals were recorded by a digital oscilloscope after being amplified. Data processing, including a 50 kHz high-pass filter and smoothing (Savizky-Golay, IR filter, of polynomial order 3), was also performed. All tests were undertaken on an aluminium bar sample whose thickness was 60 mm. Varying the generation EMAT lift-off was done through inserting plastic sheet spacers of thickness 0.1 mm between the EMAT and the sample surface, as shown in figure 7, to a maximum of 12 spacers (total lift-off of 1.2±0.1 mm).

The current output of the pulser and the impedance of the coils were measured as a function of lift-off. The inductance showed only very small variations over the lift-off range considered. The current through the coils was approximately constant over this range for all frequencies studied. No self-field generation was observed. Therefore the approximations of the generation being due to the static field, and a constant behaviour of the input current, are appropriate. The out-of-plane component of the magnetic field was measured using a Gauss meter for multiple lift-offs, and incorporated into the model via equation 7 such that the appropriate value was used for each lift-off. An approximately exponential drop off of field with lift-off was observed.

3.2. Generation EMAT configuration

Three configurations of generation EMAT were used. Each coil was near-identical, produced by hand-winding wire of diameter 0.2 mm into a loop that fitted exactly around the edge of a magnet, as shown in figure 8(a). Each coil had a width of 1.5 mm. The magnet was 25×15×18 mm, producing an out-of-plane static field in the z-direction at its centre, and coils were placed onto the magnet in the required positions and held in place using spacers. The magnetic field was predominantly in the z-direction for all coil positions. The configurations are summarised in figure 8 and described here:

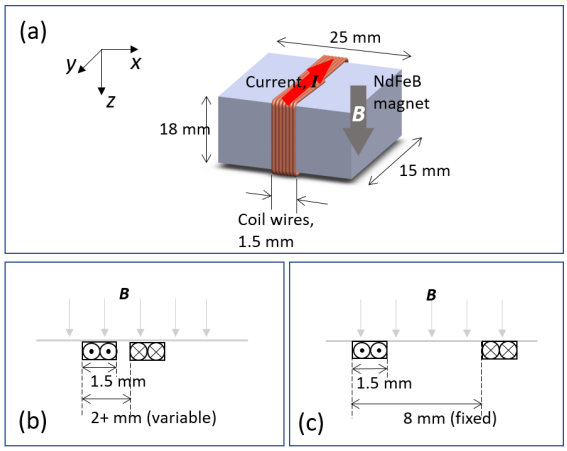

Figure 8: Generation EMAT configurations. (a) 3D sketch of the basic single coil EMAT. (b)&(c) are the cross view of the two-coil EMAT for the varied and fixed separation configurations.

- a: Single coil experiment, coil in the centre of the magnet.
- b: Two coils with currents in opposing directions with physical separationsof 2, 2.5, 3, 4 and 5 mm between coil centres. Coils were positioned equidistant from the magnet centre.
- c: Two coils with currents in opposing directions with physical separationof 8 mm, for meander (opposing) currents. Phasing was used to vary the effective separation from 2 to 5 mm.

4. Experimental results and discussion

The model was validated for a single coil, two coils (fixed separation), and two coils (phased to give an effective separation) generation. The validation quantified the change in peak frequency (shown for the calculations for a single coil in figure 4) and equivalent calculations for the two-coil set-up, and the change in amplitude of the signals with lift-off due to the changes in the mirror currents.

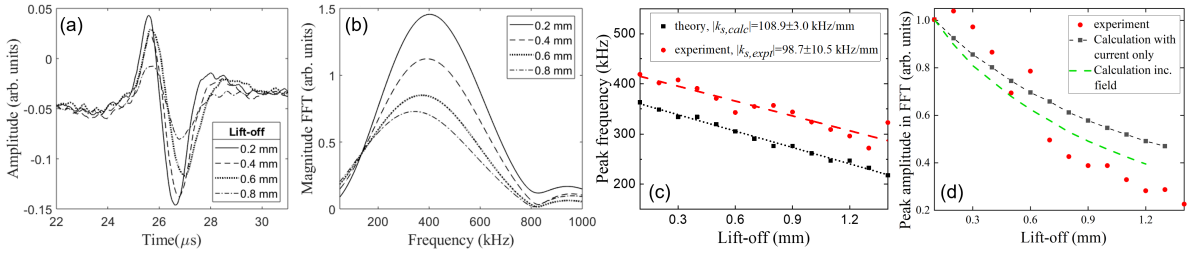

Figure 9: Lift-off for a 1.5 mm wide single coil generation EMAT. (a) Signals measured using laser interferometer, and (b) Fast Fourier transform (FFT) of the data presented in (a). (c) Compares the shift of peak frequency in the FFT of the experiment and the calculation (data shown in figure 4), while (d) compares peak magnitude.

4.1. Single coil generation with lift-off

Firstly the output from a broadband single generation coil was measured as a function of lift-off. A single cycle pulse with a frequency of 487 kHz was chosen as this gave a large signal amplitude at zero lift-off, and matches the set-up chosen for the theoretical predictions given earlier. Results from experiments are shown in figure 9(a) for lift-offs of 0.2 to 0.8 mm, showing the expected reduction in signal amplitude. Figure 9(b) shows the fast Fourier transforms (FFTs) of the data at each lift-off. A shift to lower frequencies is observed as the lift-off is increased. Since the same driving signal was used at each lift-off, this frequency shift can be explained as being primarily due to the distortion of the coil current profile shown in figure 2.

The peak frequency of the FFT is plotted as a function of lift-off in figure 9(c) for experiments and calculations with the same driving signal. The linear fit lines for experiment and calculation show a small offset of around 50 kHz, but have very similar slopes. Multiple factors contribute to this; mismatch between the simulated ideal driving frequency and the EMAT pulser output, the physical gap due to the glue and tape used to seal the coil that was not included in the measurement lift-off value, the edge variation of the permanent magnetic field etc. [29]. The slopes k, which give the rate of frequency shift with lift-off, agree well within errors, with slopes of $k_{s,expt} = 99 \pm 11$ kHz/mm and $k_{s,calc} = 109 \pm 3$ kHz/mm obtained.

Figure 9(d) shows the change in magnitude of the FFT peak, normalised to a value of one for the smallest lift-off. The model using the calculation of the current and a constant magnetic field is shown by the black points and line, while a model incorporating the measured variation of the magnetic field with lift-off is shown in green. The current-only model underestimates the change in magnitude, as expected, while the calculation including the field shows a much better prediction of the behaviour. This model does not exactly describe the behaviour, and a full model including the coil electrical behaviour and change in impedance with lift-off would show better agreement; however, this very simple model explains the majority of the change in signal amplitude for a single coil EMAT with lift-off.

4.2. Two-coil generation with lift-off

4.2.1. Time domain waveform distortion

While a single coil is broadband, when multiple coils are used in an array there is a preferred frequency which is related to the separation of the coils, although the largest signal may be obtained at frequencies slightly away from the designed wavelength shown in figure 1. Broadband pulses with a central frequency of 625 kHz were used to drive the two-coil prototype introduced in section 3 for a physical separation of 2 mm to match the calculations shown in figure 5(f) and (g). The results are shown in figure 10 for lift-offs from 0.2 to 1.0 mm. As with the single coil experiments, the signals keep a similar shape but with some distortion, and are in qualitative agreement with the calculation results shown in figure 5.

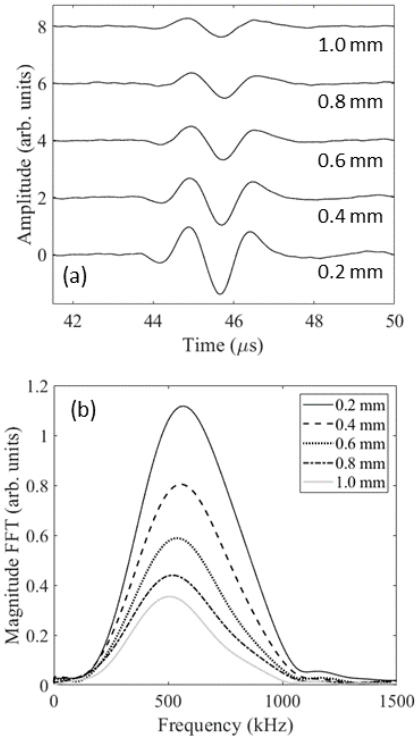

Figure 10: Lift-off for the two-coil generation EMAT for a physical coil separation of 2.0 mm, at a frequency of 625 kHz. (a) Signals measured using EMAT detector, and (b) fast Fourier transform (FFT) of the data presented in (a).

4.2.2. Comparison of physical and phased separations

The lift-off performance of a meander coil (or well separated coil array) with large d is better than that of a tightly spaced array, due to the lower frequency of operation and the behaviour of the distortions shown in figure 6 for small values of d. This section compares the behaviour of the generated ultrasound with lift-off, for two coils with differenting physical separations, or with a fixed physical separation of 8 mm but phased to have smaller effective separations.

Coil spacings of d or d_{eff} (effective coil spacing) of 2.0, 2.5, 3.0, 4.0 and 5.0 mm were tested. Each group was undertaken at lift-offs from 0.1 to 1.3 mm, where the lift-off of around 0.1 mm due to the tape protecting the coil has been included. The driving signal $y(t)$ was set for each d; the choice of centre frequency was determined by the meander-coil rule, $\lambda = 2d_{eff}$. This may not be the optimal current amplitude, but ensures a good signal-to-noise ratio for each set-up, and minimises distortion of the waveform. The corresponding frequencies were (d_{eff} : freq); 2 mm : 725 kHz, 2.5 mm : 580 kHz, 3 mm : 465 kHz, 4 mm : 350 kHz and 5 mm : 285 kHz, all calculated using a Rayleigh wave velocity of 2906 m/s [26].

Figure 11 shows the behaviour of the peak frequency with lift-off, normalised to the frequency for the smallest lift-off. The expected behaviour calculated using equations 8 and 9 is also shown. Due to the small amplitude signals obtained experimentally, there is significant scatter in the results; however, good agreement between physical and phased separations and the theoretical predictions is observed. This shows that the change in frequency behaviour is dominated by the spatial behaviour of the coils, and electrical changes have limited effects. Better lift-off behaviour is observed for wider coil separations, with the frequency of the waves remaining closer to the chosen value for zero lift-off. Bandwidth of the detector and its frequency behaviour has not been considered in this work, and will give some extra frequency-dependence to the results [14].

Peak frequency shift with lift-off is an intrinsic property of EMAT lift-off behaviour. The speed of the shift was found to further compare the perfor-

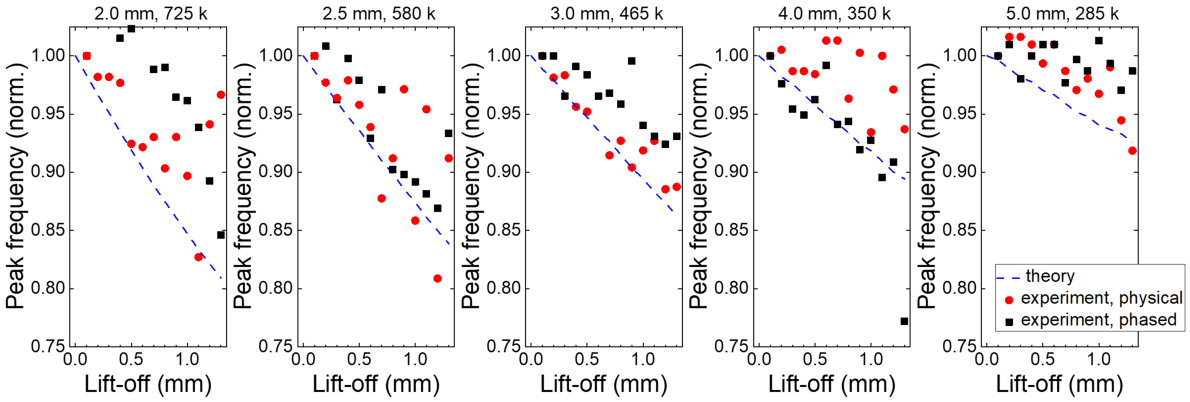

Figure 11: Peak frequency for two coil measurements, for variable physical spacings (red points), phased two-coil with fixed spacing (black points), and theoretical model (dashed lines).

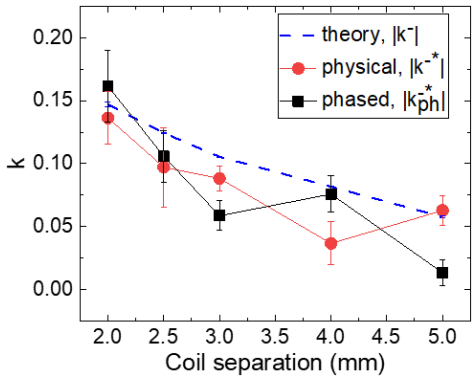

Figure 12: Slope values from linear fits to the data presented in figure 11 as a function of coil spacing. k^-, k^{-*} and k_{ph}^{-*} correspond to theory, two-coil physical, and two-coil phased, respectively.

mance between the phased pair and non-phased pair and the theoretical predictions. Linear fitting was performed for each coil spacing in figure 11. The slope of the fit was denoted k^- for the theory, k^{-*} for the physical spacing, and k_{ph}^{-*} for the phased spacing. Results are given in figure 12, again showing good agreement between the physical and phased separations, and the theoretical predictions.

Figure 13 shows the magnitude of the peak in the FFT with lift-off for each separation, for variable physical spacings (red points), phased two-coil with fixed spacing (black points), and the theoretical model. As with the single coil, the magnitude change has been calculated for a constant magnetic field (blue dashed lines) and for the measured field with lift-off combined with equation 7. Factors affecting the behaviour include the spatial spreading and lift-off dependence included in the theory, the reduction in the magnetic field strength with lift-off, changes in impedance, electrical interaction between the two coils, and the divergence of the magnetic field.

The experimental data for phased and physical spacing match well for the larger separations, with a clear disagreement only for the smallest spacing tested. The agreement in the data for larger values of d and d_{eff} shows that there are minimal electrical interactions between the coils, and that the field divergence effect is small. For the smallest physical separations the effect of coil interaction must also be considered, accounting for the disagreement between phased and physical results. Where very high frequency (small d) operation is required, using coils with a large physical separation and phasing them to give a small effective separation may be beneficial, but the benefits to the lift-off behaviour are limited. The model fits very well to the data for small separations, accurately predicting the lift-off behaviour when the magnetic field change is taken into account. There are some disagreements at larger separations, where the model suggests that better lift-off perfor-

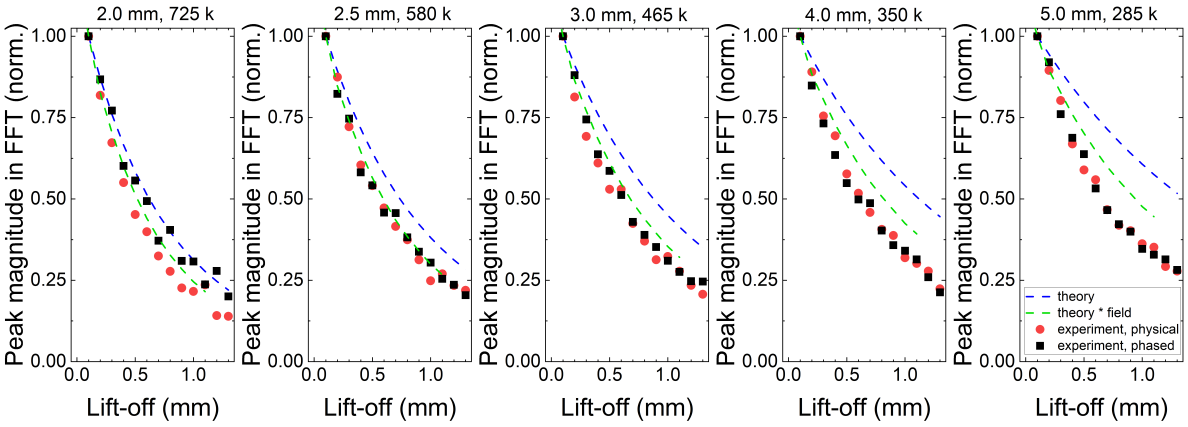

Figure 13: Magnitude of the FFT peak for two coil measurements, for variable physical spacings (red points), phased two-coil with fixed spacing (black points), and theoretical model with constant field (blue dashed lines) or measured field (green dashed lines).

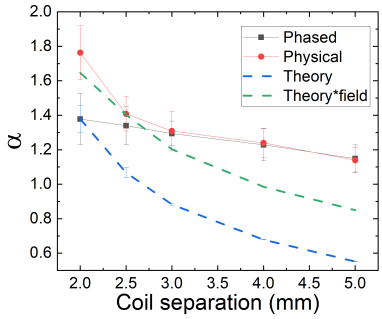

Figure 14: Exponential fits to the data in figure 13.

mance is expected.

Figure 14 shows exponential fit values α, when $f(h) = A\exp[\alpha h] + f_0$ is fit to the FFT magnitudes in figure 13, for all experimental data and calculations. As before, the prediction from the calculations with fixed magnetic field underestimates the decay in all cases, while when including the measurement of magnetic field agreement is improved, but the behaviour is not fully modelled using the very simple model presented in this paper. This may be due to conflict between the meander coil "rule of thumb" and the coil width frequency influence [14] used when choosing the frequency of operation, or potentially due to further influence from the coil electrical behaviour. This will be investigated in future work.

5. Conclusions

The calculations and experiments within this paper show that, for a full understanding of the lift-off behaviour of an EMAT, the spatial behaviour must be considered alongside the electrical behaviour, and will in fact dominate the frequency behaviour. Due to the finite size of the EMAT coil, the transmitted electromagnetic fields are distorted as lift-off increases, and will therefore significantly affect the ultrasonic behaviour.

Studies on the single linear coil EMAT has shown that, for a 1.5 mm width linear coil, the peak frequency of the generated Rayleigh wave decreased at a rate of around 100 kHz/mm with lift-off. Good agreement was observed between the analytical prediction of the frequency behaviour and experimental results. This shift needs to be considered if an experiment is designed to be done at a chosen frequency or range of frequencies and lift-off is likely to vary. The spatial model also describes well the change in signal amplitude with lift-off for the single coil.

The study of the behaviour of an EMAT coil array was undertaken via a two-coil model. The effective region of each single coil element is broadened

as lift-off is increased, and the spatial changes due to the interaction between the currents generated by neighbouring coils cannot be neglected. Again, experiments and calculations for the shift in peak frequency agree very well, with the phased and physical separations shown to be equivalent within noise levels for all but the smallest physical coil separations. The simple analytical model suggests that the shape effect which governs the frequency behaviour is primarily due to the coil size and lift-off, and also dominates the amplitude behaviour. When considering the amplitude changes there will also be some dependence on the material's electromagnetic properties. This may be of interest where the self-field generation mechanism is stronger.

In order to obtain high frequencies from a meander coil, one needs the turns in the coil to be very closely spaced. This can lead to interactions between the currents in the different parts of the coil. By using an array and separating the coils physically, while using phasing to make them appear to be closer, one can obtain higher frequencies in a simpler fashion [18]. However, this work has shown that the behaviour with lift-off continues to be dominated by the effective spatial force distribution spread for each coil in the array, and the benefits to operating at higher lift-offs are only found for very small separations / high frequencies. These results suggest that, for the design of an array EMAT, a good lift-off performance always conflicts with the need for high frequency narrowband operation. This trade-off must always be considered when designing an experiment. Should a better performance be required, using more coils would give a more narrowband behaviour which could improve lift-off performance – however, the current spread underneath each coil will remain the same.

Reference [14] gave a design parameter that could be used to predict the frequency at which a race-track coil will operate; there is not such a simple one-equation-fits-all approach from this work as it depends on which frequency is required and what material is used. Further work will look at how the distortion effect can be decreased using other considerations, for example using a ferrite backing or other ways to focus the magnetic energy.

References

[1] M. Hirao, H. Ogi, Electromagnetic Acoustic Transducers: Noncontacting Ultrasonic Measurements using EMATs, Springer (2017).

[2] R. B. Thompson, Physical principles of measurement with EMAT transducers, Physical Acoustics 19 157–200 (1990).

[3] C. V. Dodd, W. E. Deeds, Analytical solutions to eddy-current probe-coil problems, Journal of Applied Physics 39(6) 2829 (1968).

[4] N. Lunn, S. Dixon and M. D. G. Potter, High temperature EMAT design for scanning or fixed point operation on magnetite coated steel, NDT&E International 89 74–80 (2017).

[5] F. Hernandez-Valle, A. R. Clough and R. S. Edwards, Stress corrosion cracking detection using non-contact ultrasonic techniques, Corrosion Science 78 335–342 (2014).

[6] R. S. Edwards, S. Dixon and X. Jian, Characterisation of defects in the railhead using ultrasonic surface waves, NDT&E International 39(6) 468–475 (2006).

[7] A. V. Clark, Y. Berlinsky, Effect of liftoff on accuracy of phase velocity measurements made with electromagnetic-acoustic transducers, Journal of Research in Nondestructive Evaluation 4:2 79–96 (1992).

[8] J. P. Morrison, S. Dixon, M. D. G. Potter, X. Jian, Lift-off compensation for improved accuracy in ultrasonic lamb wave velocity measurements using electromagnetic acoustic transducers (EMATs), Ultrasonics 44 1401–1404 (2006).

[9] S. Huang, W. Zhao, Y. Zhang, S. Wang, Study on the lift-off effect of EMAT, Sensors and Actuators A: Physical 153 218–221 (2009).

[10] P. Yi, K. Zhang, Y. Li, X. Zhang, Influence of the lift-off effect on the cut-off frequency of the EMAT-generated Rayleigh wave signal, Sensors 14 (10) 19687–19699 (2014).

[11] W. Shi, Y. Wu, H. Gong, T. Zhang, L. Tan, L. Han, J. Yang, W. Li, Optimal design of spiral coil electromagnetic acoustic transducers considering lift-off sensitivity operating on non-ferromagnetic media, Nondestructive Testing and Evaluation 33 (1) 56–74 (2018).

[12] P. Petcher, M. Potter, S. Dixon, A new electromagnetic acoustic transducer (EMAT) design for operation on rail, NDT & E International 65 1–7 (2014).

[13] X. Jian, S. Dixon, R. S. Edwards, J. Reed, Coupling mechanism of electromagnetic acoustic transducers for ultrasonic generation, The Journal of the Acoustical Society of America 119 2693 (2006).

[14] C. B. Thring, S. J. Hill, S. Dixon, R. S. Edwards, The effect of EMAT coil geometry on the Rayleigh wave frequency behaviour, Ultrasonics 99 105945 (2019).

[15] S. Wang, R. Su, X. Chen, L. Kang, G. Zhai, Numerical and experimental analysis of unidirectional meander-line coil electromagnetic acoustic transducers, IEEE Transducers on Ultrasonics, Ferroelectrics, and Frequency Control 60 2657 (2013).

[16] C. Pei, S. Zhao, P. Xiao, Z. Chen, A modified meander-line-coil EMAT design for signal amplitude enhancement, Sensors and Actuators A: Physical 247 539–546 (2016).

[17] G. Zhai, Y. Li, Y. Qin, Y. Liu, Design Method of Multiwavelength EMATs Based on Spatial Domain Harmonic Control, IEEE Transactions on Ultrasonics, Ferroelectrics, and Frequency Control, 68 (6) 2259–2270 (2021).

[18] L. Xiang, D. Greenshields, S. Dixon, R. S. Edwards, Phased electromagnetic acoustic transducer array for Rayleigh wave surface defect detection, IEEE Transactions on Ultrasonics, Ferroelectrics, and Frequency Control 67 1403–1411 (2020).

[19] J. Tkocz, S. Dixon, Electromagnetic acoustic transducer optimisation for surface wave applications, NDT & E International 107 102142 (2019).

[20] H. J. Tsaknakis, E. E. Kriezis, Field distribution due to a circular current loop placed in an arbitrary position above a conducting plate, IEEE Transactions on Geoscience and Remote Sensing GE-23 (6) 834–840 (1985).

[21] S. M. Panas, A. G. Papayiannakis, Eddy currents in an infinite slab due to an elliptic current excitation, IEEE Transactions on Magnetics 27 (5) 4328–4337 (1991).

[22] S. H. H. Sadeghi, A. H. Salemi, Electromagnetic field distributions around conducting slabs, produced by eddy-current probes with arbitrary shape current-carrying excitation loops, IEE Proceedings - Science, Measurement and Technology 148 (4) 187–192 (2001).

[23] T. Theodoulidis, Analytical model for tilted coils in eddy-current nondestructive inspection, IEEE Transactions on Magnetics 41 (9) 2447–2454 (2005).

[24] X. Jian, S. Dixon, K. T. V. Grattan, R. S. Edwards, A model for pulsed Rayleigh wave and optimal EMAT design, Sensors & Actuators A 128 296–304 (2006).

[25] R. R. Hughes, High-sensitivity eddy-current testing technology for defect detection in aerospace superalloys, Ph.D. thesis, University of Warwick (2015).

[26] G. W. C. Kaye, T. H. Laby, Tables of physical and chemical constants, 16th Edition, Harlow:Longman (1995).

[27] P. Khalili, P. Cawley, Relative ability of wedge-coupled piezoelectric and meander coil EMAT probes to generate single-mode Lamb waves, IEEE Transactions on Ultrasonics, Ferroelectrics, and Frequency Control 65 (4) 648–656 (2018).

[28] M. Klein, G. B. GD, A. G.-J. A, D. Wright, W. Moerner, Homodyne detection of ultrasonic surface displacements using two-wave mixing in photorefractive polymers, Optics Communications 162 79–84 (1999).

[29] Y. Fan, S. Dixon, X. Jian, Lift-off performance of ferrite enhanced generation EMATs, AIP Conference Proceedings 975 (1) 835–840 (2008).